



High pressure X-ray emission spectroscopy at the advanced photon source

Yuming Xiao, Paul Chow & Guoyin Shen

To cite this article: Yuming Xiao, Paul Chow & Guoyin Shen (2016) High pressure X-ray emission spectroscopy at the advanced photon source, High Pressure Research, 36:3, 315-331, DOI: [10.1080/08957959.2016.1209498](https://doi.org/10.1080/08957959.2016.1209498)

To link to this article: <http://dx.doi.org/10.1080/08957959.2016.1209498>



Published online: 22 Jul 2016.



Submit your article to this journal [↗](#)



Article views: 44



View related articles [↗](#)



View Crossmark data [↗](#)

High pressure X-ray emission spectroscopy at the advanced photon source

Yuming Xiao, Paul Chow and Guoyin Shen

HPCAT, Carnegie Institution of Washington, Argonne, IL, USA

ABSTRACT

The structural, electronic, and magnetic properties of materials under high pressure are of fundamental interest in physics, chemistry, materials science, and earth sciences. Among several hard X-ray-based techniques, X-ray emission spectroscopy (XES) provides a powerful tool to probe element-specific information for understanding the electronic and magnetic properties of materials under high pressure. Here, we discuss on the particular requirements and instrumentation used in high pressure XES experiments. We then present several examples to illustrate the recent progress in high pressure XES studies at the Advanced Photon Source, followed by an outlook toward future development in high pressure XES.

ARTICLE HISTORY

Received 29 April 2016
Accepted 1 July 2016

KEYWORDS

High pressure; X-ray emission spectroscopy; synchrotron radiation

1. Introduction

In high pressure X-ray emission spectroscopy (XES), high-energy X-rays are used to excite deep-core electrons in the sample embedded within high pressure vessels. The high-energy X-rays provide the necessary penetrating power for photons to pass through thick surrounding materials (anvils, gaskets) of the pressure vessel. The subsequent fluorescence radiation, typically collected through X-ray transparent materials (e.g. beryllium), provides information on the occupied electronic states of the sample, such as the core-level binding energies and the valence-band density of states. It is a powerful hard X-ray probe for studying element-specific electronic and magnetic properties of materials. Since the late 1990s, XES has been widely used to study the behavior of materials under high pressure.[1–3]

XES is a second-order process, as illustrated in Figure 1. A core electron is excited by the incident X-ray photons; subsequently, the core hole is filled by an electron from a higher shell, accompanied by emitting a photon during the process. The energy of the emitted photon is equal to the energy difference between the two electronic levels. This process can be described using the Kramers–Heisenberg equation under the hard X-ray approximation (non-coherent process) [4]

$$F(\omega_1, \omega_2) = \sum_f \sum_n \frac{\langle f | \hat{H}_{\text{int}} | n \rangle^2 \langle n | \hat{H}_{\text{int}} | i \rangle^2}{(E_i - E_n + \hbar\omega_1)^2 + \Gamma_n^2/4} \times \frac{\Gamma_f/2\pi}{(E_i - E_f + \hbar\omega_1 - \hbar\omega_2)^2 + \Gamma_f^2/4} \quad (1)$$

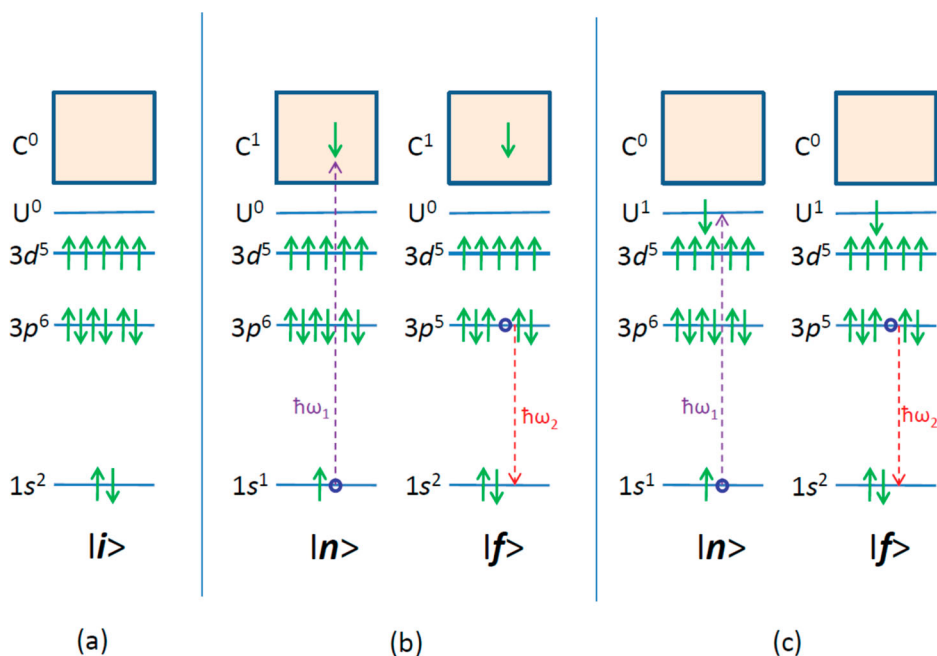


Figure 1. Illustration of XES and RXES processes using $K_{\beta_{1,3}}$ emission of high-spin Mn^{2+} . (a) The initial state $|i\rangle$; (b) non-resonant and (c) resonant XES process. U and C indicate the unoccupied levels and the continuum, respectively. The purple arrows represent the absorption of an incoming photon of energy $\hbar\omega_1$ to either the continuum or the resonant intermediate state $|n\rangle$, and the red arrows indicate the decay of an electron from a higher level to the core hole with final state $|f\rangle$ accompanied by the emission of a photon of energy $\hbar\omega_2$. The $K_{\beta'}$ peak comes from the interaction between the $3p$ core hole and the partially filled $3d$ electrons.

where $\hbar\omega_1$ and $\hbar\omega_2$ are the incident and emitted photons, respectively and E_i , E_n , and E_f are the energies of the initial, intermediate, and final states. Γ_n and Γ_f are the lifetime broadening associated with the intermediate and final states.

When the incident photon energy is high enough to excite the electron from core level and not nearby an absorption edge, this emission process is called non-resonant emission, which is independent of the incident X-ray energy. The emission line is named after the energy level of the electron which fills the core hole generated by the incident photon. As an example, the K-shell emission lines of Fe, i.e. the photons that are emitted after creation of a hole in the $1s$ shell, are shown in Figure 2. Transitions from the $2p_{3/2}$ and $2p_{1/2}$ levels are called K_{α_1} and K_{α_2} and their intensities are the strongest among K emission lines. Spectral changes of K_{α} lines are usually very small and there is a linear relation between the full-width-half-maximum (FWHM) of K_{α_1} emission peak of $3d$ transition metal and spin state of the metal ion.[5] Due to their high intensities, K_{α} lines are often used in partial fluorescence yield (PFY) measurements. $K_{\beta_{1,3}}$ lines are transitions from the $3p$ levels and are usually one order of magnitude weaker than K_{α} lines. Due to the exchange interaction between $3p$ and $3d$ electrons, there is a small peak called $K_{\beta'}$ on the lower energy side of $K_{\beta_{1,3}}$ main peak. $K_{\beta_{1,3}}$ and $K_{\beta'}$ together are called K_{β} main lines. Oxidation state and spin state information can be obtained from the K_{β} main lines. Transitions from valence levels are termed K_{β} satellite lines ($K_{\beta_{2,5}}$ and $K_{\beta''}$), also known as valence-to-core emission

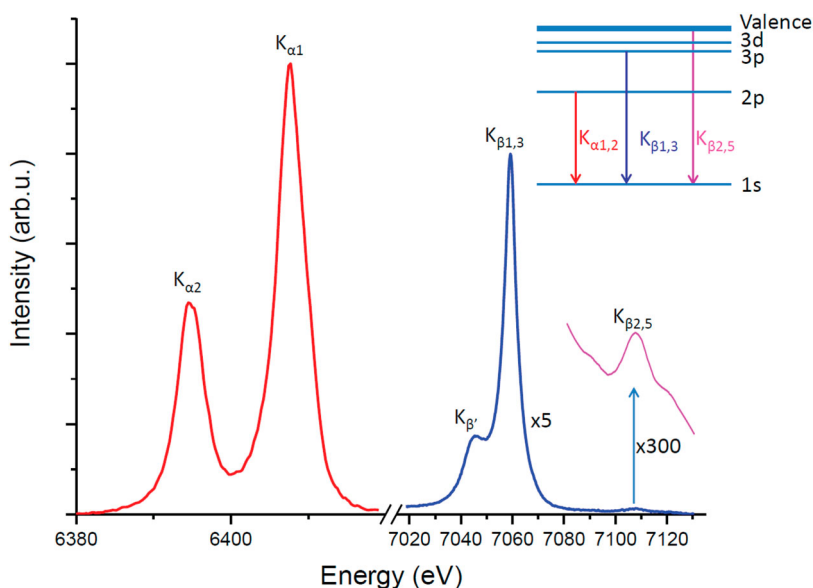


Figure 2. The K-shell emission line in Fe₂O₃ and a schematic drawing of the transitions (see text for details).

lines. Intensities of the K_β satellite lines are even weaker compared to K_β main lines due to less overlap between wave functions of initial and final states. Since the K_β satellite lines originate from valence electron levels, they can be used to identify ligands which have close atomic numbers and characterize valence electronic levels.[6]

When an incident photon energy is tuned across an absorption edge of the element of interest, the emission process is called the resonant emission. Resonant XES (RXES) may be viewed as a combination of X-ray absorption spectroscopy (XAS) and XES. Distinct from non-resonant XES, RXES spectra are often dependent on the incident X-ray energy. Instead of collecting transmitted X-rays or total fluorescence yield as in XAS, emission spectra are measured at each step as the incident beam energy is changed across an absorption edge. Therefore, the emission signal can be collected in a 2D map of the incident energy vs. emission energy. The projection of the incident and emission planes gives the PFY and RXES, respectively. Because the lifetime broadening of the final state is considerably smaller than that of the core excited state, this resonant method significantly enhances footprints of electron states, and has a remarkable sharpening effect in the PFY spectra.

PFY is essentially an XAS probe providing information on the oxidation state, coordination state, and electronic structure of the absorbing element.[3] PFY spectra were first reported by Eisenberger et al. and has been extensively used since the 1990s with the advent of third-generation synchrotron sources.[7] The sharpening effect in the PFY is clearly beneficial in studying 3d transition metal, lanthanide and actinide systems, often using K_α or L_α lines due to their strong signals in XES. Figure 3 is an example of YbCoIn₅ at 56 GPa. The RXES plane was measured around the Yb L_{III} edge at 8.944 keV, by measurement of the L_{α1} X-ray emission at 7.415 keV (3d_{5/2} → 2p_{3/2} core-to-core transition). The top panel of Figure 3 shows a projected PFY – XANES spectrum at the fixed energy of

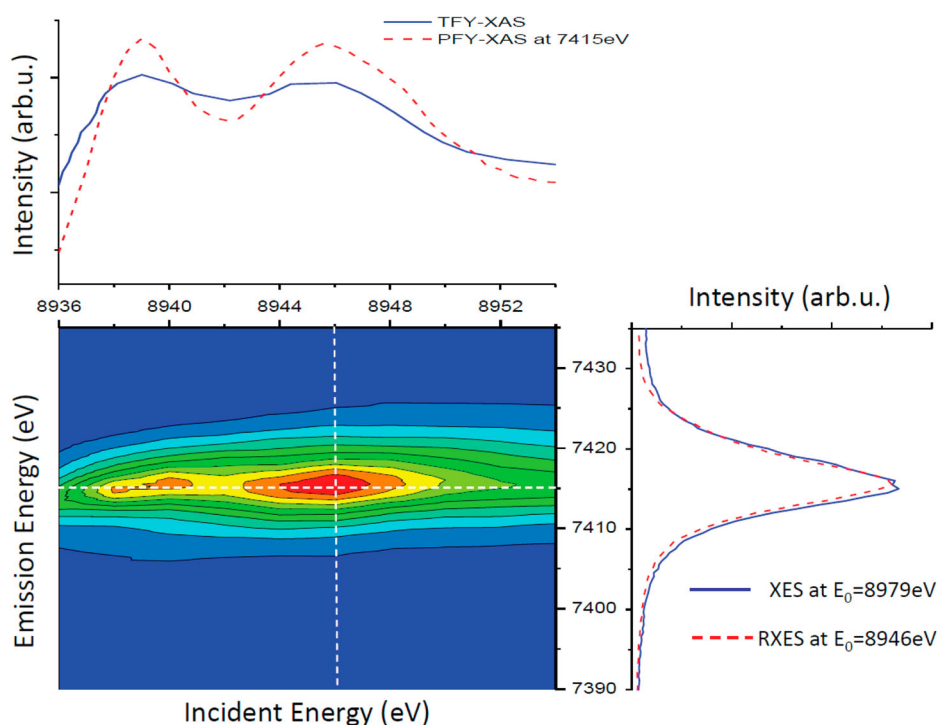


Figure 3. $L_{\alpha 1}$ RXES plane of YbCoIn_5 around the Yb L_{III} absorption edge at 56 GPa. Right: Resonant (red dashed line) and non-resonant (blue solid line) XES spectra. Top: PFY-XAS (red dashed line) and TFY-XAS extracted from ref. [59] (blue solid line) spectra.

7.415 keV. A remarkable sharpening effect is visible, with two clear peaks corresponding to Yb^{2+} and Yb^{3+} configurations. The right panel shows two XES spectra measured at 8.946 keV (red dashed line) and 8.979 keV (blue line). There is no general sharpening effect when XES spectra measured around resonance energies are compared to those measured at non-resonant energies. The spectrum measured at 8.946 keV is slightly narrower than the spectrum measured at 8.979 keV due to a maximum in the XAS spectrum at the excitation energy of 8.946 keV. Depending on the shape of density of states at the particular excitation energy, the width of XES spectrum measured around absorption edge can be narrower or broader than that measured non-resonant, as discussed in detail by de Groot et al.[8,9]

2. High pressure XES instrumentation

High-energy resolution XES experiments have been carried out since the 1970s. However, XES experiments under high pressure started only in the late 1990s due to the requirements and challenges of high pressure experimental conditions.[1] First of all, sizes of high pressure samples are small. Depending on the target pressure of the experiment, sample size ranges from tens of micrometers to a few hundreds of micrometers in diameter and sample thicknesses are even less, normally just a few micrometers to a few tens of micrometers. To get acceptable signal-to-noise ratios with such small samples, a tightly

focused and extremely intense beam becomes necessary for high pressure XES experiments. Secondly, in order to generate high pressure conditions, the sample is always surrounded by other materials, such as gaskets, anvils, and the pressure medium. The volume of these surrounding materials is several orders of magnitude larger than that of the sample giving rise to overwhelming background scattering. A beryllium gasket is mostly used in high pressure XES experiments with diamond anvil cells (DACs). In order to minimize the scattering background, the analyzer of an XES spectrometer is usually set perpendicular to the incident beam and a clean focused beam smaller than sample size should be used to avoid contribution to the measured signal from impurities in the gasket. Due to the weak sample signal and strong background scattering, collimation becomes critical in high pressure XES experiment. On the detector side, a collimation slit needs to be used to make sure that the detector receives only diffracted photons from the analyzers. On the sample side, a confocal optics like a half-lens polycapillary can help to collect the emission signal only from the sample region. Thirdly, different experimental geometries can be selected depending on experimental requirements. In Figure 4, we plot the energy-dependent absorption curves for the transverse geometry (the incident X-rays go through one diamond anvil and the emission signal comes out from the Be gasket) and the in-plane geometry (the incident X-ray goes in and out through the Be gasket) for two incident energies (11.6 keV for non-resonant Fe XES and 7.112 keV for Fe RXES). By taking into account the undulator flux and the diamond absorption, we usually select the incident energy around 11.6 keV at HPCAT for most non-resonant XES experiments.[10] From the absorption efficiency point of view, the in-plane geometry is

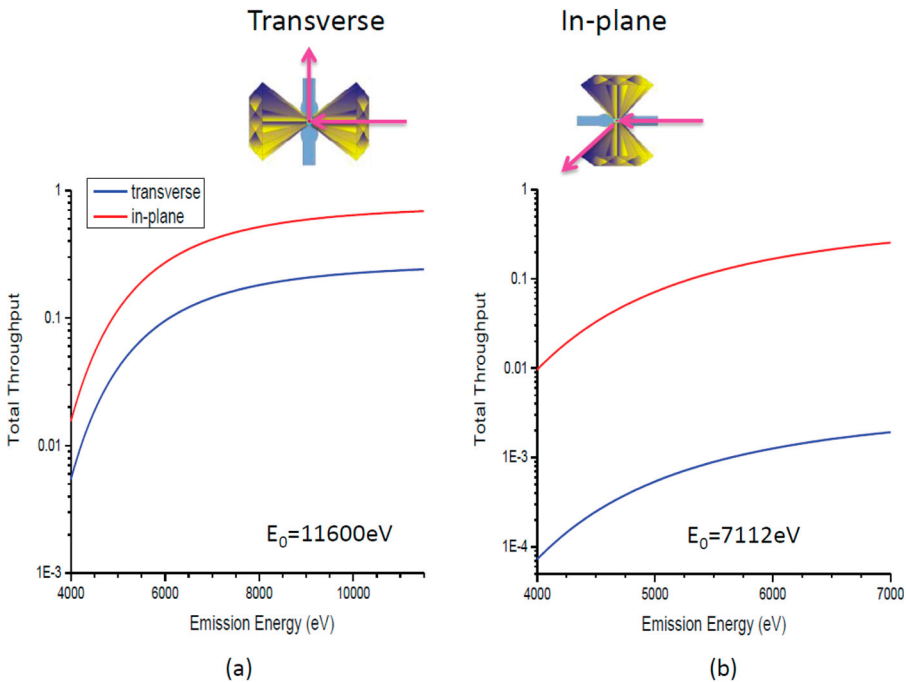


Figure 4. Total throughput curves for transverse geometry (blue) and in-plane geometry (red) for two different incident X-ray energies: (a) 11,600 eV and (b) 7112 eV.

preferred. However, the transverse geometry is often used when the incident X-ray energy is above 10 keV because this geometry is relatively simple to be integrated with other *in situ* measurements such as an online Ruby instrument for *in situ* pressure measurement and integration with X-ray diffraction (XRD). Another important reason for the transverse geometry is that the Be gasket normally has impurities (Fe, Cu etc.), which may contaminate the sample signal. Also for the transverse geometry, the beam needs to go through the Be gasket, but only once. When there is pressure gradient in the sample, having incident X-rays parallel to the loading axis in the transverse geometry is the preferred way to minimize the gradient effect. For RXES experiments that require incident energies below 10 keV, the in-plane scattering geometry is then used due to strong diamond absorption.

Depending on the application and energy range of interest, various XES spectrometers can be employed. In Figure 5, schematic drawings of four different spectrometer designs are shown and discussed below.

2.1. XES using spherically bent analyzers

In this spectrometer design, the sample position, the analyzer, and the detector are in the Rowland circle geometry. For different emission energies, the Rowland condition is achieved by adjusting the distances between analyzer and sample, and analyzer and

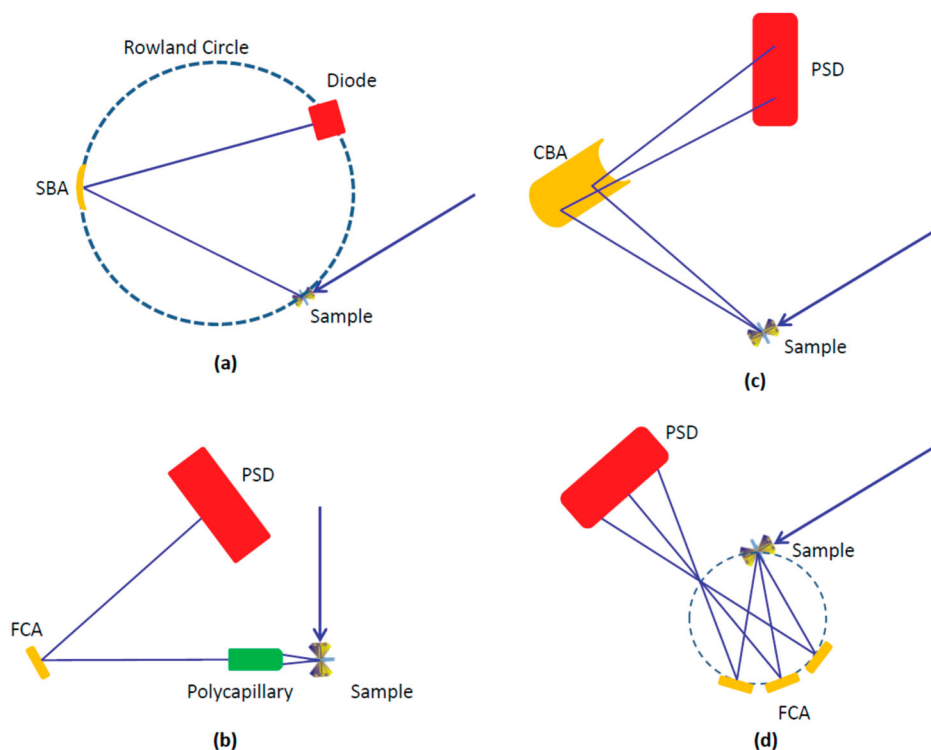


Figure 5. Schematic drawings of four XES spectrometer designs. (a) Spherically bent analyzer (SBA); (b) polycapillary half-lens, FCA: flat crystal analyzer, PSD: position-sensitive detector; (c) von Hamos geometry, CBA: cylindrically bent analyzer; and (d) miniature XES spectrometer.

detector. An emission spectrum is obtained by rotating the analyzer $\Delta\theta$, tracked by the corresponding $2\Delta\theta$ rotation of the detector. This spectrometer geometry is most commonly used and has been implemented in many beamlines around the world. In order to increase the collected solid angle, spectrometers with multiple analyzers were built.[11–13]

2.2. XES using a polycapillary half-lens

A polycapillary lens can be used as a confocal optic to reduce background scattering from materials surrounding the sample within high pressure devices. Another advantage of using a polycapillary lens is its large solid angle of collection. The polycapillary lens is aligned close to the sample ($\sim 5\text{--}10$ mm depending on the DAC and optics designs) and collects the emitted emission signal. One or two small flat crystals are used as an analyzer for the quasi-parallel output beam (~ 10 mm in size) from the polycapillary half-lens. A detector collects the diffracted beam from the flat crystal.

Szlachetko et al. used the double-crystal geometry giving a spectrometer energy resolution of ~ 2 eV at 6.4 keV.[14] The two crystals are arranged in a dispersive (+n, +n) configuration. The second crystal passes only photons that fulfill the Bragg criteria. The double-crystal setup can be employed for analyzers with relatively small Bragg reflection angles. Special cut analyzers are not needed. However, the intensity is reduced by a factor of ~ 20 due to the second Bragg reflection. Mortensen et al. built a simplified polycapillary-based XES spectrometer specifically for high pressure studies of 4f-electron systems using one flat crystal working close to backscattering geometry.[15] The typical energy resolution was $\sim 5\text{--}10$ eV, which is suitable for studies of 2p excitation of lanthanides because of the comparable core-hole lifetime broadening of the excitation (about 4–5 eV).

2.3. XES based on the von Hamos geometry

In the above-mentioned two geometries, the energy spectrum is angularly dispersed and requires scanning the crystal analyzer. The XES spectrometer based on the von Hamos geometry can record an XES spectrum on a single-shot basis. The major components of the XES spectrometer are a cylindrically bent crystal and a position-sensitive detector. As illustrated in Figure 5(c), the cylindrically bent crystal diffracts the fluorescence from the sample to the position-sensitive detector and generates a 2D image. The energy of the emission photon is determined by its position on the detector along the axis of dispersion. The energy bandwidth covered by the spectrometer can be a few tens to a few hundreds of eV's and is set primarily by the length of the crystal and size of the position-sensitive detector.[16] The bending radius of the analyzer crystal, source size, and detector pixel size are the main factors determining the energy resolution and collection efficiency of the spectrometer. A spectrometer based on the von Hamos geometry has better intrinsic energy resolution compared to spectrometer using spherically bent crystal if the same bending radius is used, due to less lattice strain in a cylindrically bent crystal compared to a spherically bent crystal.

XES spectrometers with the von Hamos geometry have been used in plasma diagnostics and ion-impact-generated X-ray spectra in the 1980s.[17] Hoszowska *et al.* later built a high-resolution von Hamos Bragg crystal XES spectrometer to study XES in the range of

1.5–15 keV; the spectrometer was used with both laboratory and synchrotron X-ray sources.[18] With the improvement of position-sensitive detectors and availability of very intense X-ray pulses generated by the XFEL source, spectrometers with the von Hamos geometry have gained more and more attention in recent years due to their single-shot capacity, which enables time-resolved applications of XES.[19,20]

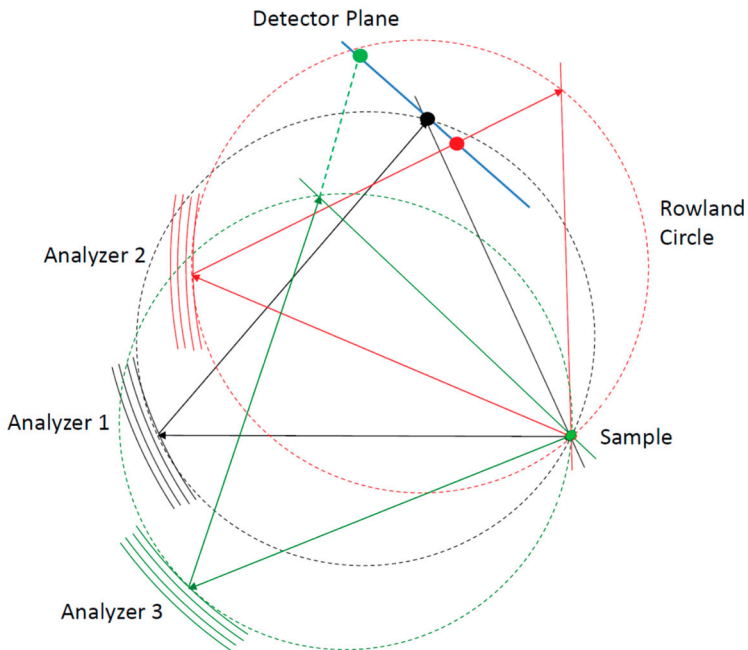
2.4. Miniature XES spectrometer

Similar to the spectrometer with the von Hamos geometry, a miniXES spectrometer uses a position dispersive arrangement. It contains a few small flat crystals which are placed close to the sample and arranged in a spherically curved surface, together with a spatial filtering aperture and a low-noise X-ray position-sensitive (area) detector as illustrated in [Figure 5](#) (d). Due to its close proximity to the sample, a large solid angle of XES signal from the sample can be collected. Collection of solid angles of existing miniXES spectrometers can be as large as 0.14 sr depending on the design, comparable to that of ~ 17 spherically bent crystal analyzers (SBCA) at 1 m working distance. A miniXES spectrometer has several unique advantages compared to the generally large physical scale and high construction cost of XES spectrometers with SBCA. They are easy to make, inexpensive and can be portable and shared with many beamlines. However, the energy range covered by a miniXES spectrometer is narrow; one spectrometer usually is designed for only one emission line and data analysis is not trivial for general users. Energy calibration for each individual pixel of the position-sensitive detector and image processing is required. For very dilute samples under Mbar pressure with a very low signal count rate, the background may become an issue for the image processing required in data analysis. Several miniXES spectrometers have been built for various applications.[21,22] Among them, one was specifically built to study Pr metal and its compounds under high pressure by Pacold et al.[23]

From the general user operation point of view, the XES spectrometer with spherically bent analyzers is still the main workhorse in XES experiments at synchrotron beamlines. To increase collection solid angle, multiple analyzers are used and usually all analyzers lie in the same horizontal plane. However, the DACs for HP studies usually have a limited access opening. For example, the most commonly used 2-inch symmetric cell at HPCAT has an opening cone angle of $\sim 15^\circ$. A 4-inch bent crystal analyzer with 1 m radius covers $\sim 5^\circ$. Efficient collection requires a DAC with at least a 35° opening if the XES spectrometer has seven analyzers arranged horizontally. To address this issue, we are in the process of building a seven-analyzer XES spectrometer with analyzers arranged in conical geometry. Seven analyzers will be arranged in three rows with three analyzers in the middle row and two analyzers in the upper and lower rows, as illustrated in [Figure 6](#)(a). We use three analyzers arranged vertically to explain the design concept because the spectrometer design with only multiple horizontal analyzers has been discussed in detail before.[11–13] To add more analyzers in the vertical plane, analyzer 2 and 3 can be treated as analyzer 1 rotated about the sample point as shown in [Figure 6](#)(b). A position-sensitive area detector is needed with this design because analyzers at different vertical levels focus the beam to different positions on the detector in order to fulfill a common Bragg angle condition as represented by green, black, and red dots in the detector plane shown in [Figure 6](#)(b). To minimize the separation on the detector for different



(a)



(b)

Figure 6. (a) Photograph of seven analyzers arranged in conical geometry; (b) schematic drawing of three analyzers arranged vertically and their Rowland circles, respectively.

rows, it is preferred to use analyzer indices so that the detector is as close to backscattering as possible. Depending on the Bragg angle, the separation can be large (a few tens of millimeters); thus good collimation for the detector active area is very critical to improve signal-to-noise ratios. In order to minimize setup for analyzer switching and alignment, for each analyzer module, we plan to motorize two angles and one radial translation. Our goal is to align all seven analyzers in 3–4 h with automatic scanning macros.

3. High pressure XES applications

3.1. 3d transition metals

Among the many interesting problems in the 3d transition metal physics, understanding the spin state of metals is of paramount importance due to its correlation with many other material properties, such as structure, thermodynamics, and bonding. Because of the interactions between 3d electrons and the 3p core hole, K_{β} mainline XES of 3d transition metals is an effective local and bulk probe for the magnetic spin moment and has been applied to study spin transitions of many transition metal oxides, strongly correlated materials and mantle minerals under high pressure.[24–27] Since the discovery of iron-based superconductors in 2008, one of the debated questions is the duality of the local moment-itinerant electron in magnetism.[28] There were many studies of local magnetic moments in various Fe-based superconductors under high pressure using Fe K_{β} XES, some of which were also at low temperature to study the superconducting state.[29–31]

In order to understand how structural and magnetic degrees of freedom affect superconductivity, the so-called 122 compounds AFe_2X_2 (where A is an alkaline-earth element, an alkali metal or Eu and X is a pnictogen element) have been extensively studied. As an example, Figure 7 shows room temperature and high pressure XES spectra of $(Ca_{0.67}Sr_{0.33})Fe_2As_2$ at 1.5 and 6.6 GPa.[29] The parent compound has antiferromagnetic order at ambient pressure, and chemical substitutions can suppress magnetism and induce superconductivity. Sr substitution into $CaFe_2As_2$ can decouple the quenching Fe local moment from the volume collapse transition. A small single crystal was loaded into a DAC with a 3 mm Be gasket, using silicone oil as the pressure medium. To extract the Fe local moment, the integrated absolute difference method was used and the XES spectrum at 0.1 GPa was measured as ref. [32] The difference spectra (shown in solid gray lines) grow larger with increasing pressure: a shift to lower energy of the main peak and a very small loss of spectral weight in the $K_{\beta 1,3}$ region around 7045 eV are observed, indicating a reduction in the Fe moment. HP XES results reveal that the Fe moments persist into the collapsed-tetragonal (CT) structure. Results of XRD and XES measurements show that the CT phase of $(Ca_{0.67}Sr_{0.33})Fe_2As_2$ can support a substantial Fe moment that appears to be strongly coupled to the *c*-axis lattice parameter, which is controlled by the size of the alkaline-earth atom, thermal contraction, and the volume change induced by the CT phase.

3.2. Lanthanides and actinides

The lanthanide and actinide elements share very similar physical and chemical behavior and show many interesting phenomena, such as heavy-fermion metals properties, and intermediate valence and unconventional superconductivity due to their *f* electrons.[3,33–35] However, whereas 4*f* electrons in lanthanides are generally more localized and close to the atomic core, the 5*f* electrons in actinides are more extended, itinerant and interact strongly with neighboring ligand orbitals and the conduction band. External pressure can affect the hybridization of *f*-electrons and alter crystallographic, magnetic and transport properties of these materials dramatically. The application of *ab initio* calculations to *f*-electrons still remains a considerable challenge and experimental data on critical quantities such as the local magnetic moment and valence are much needed to

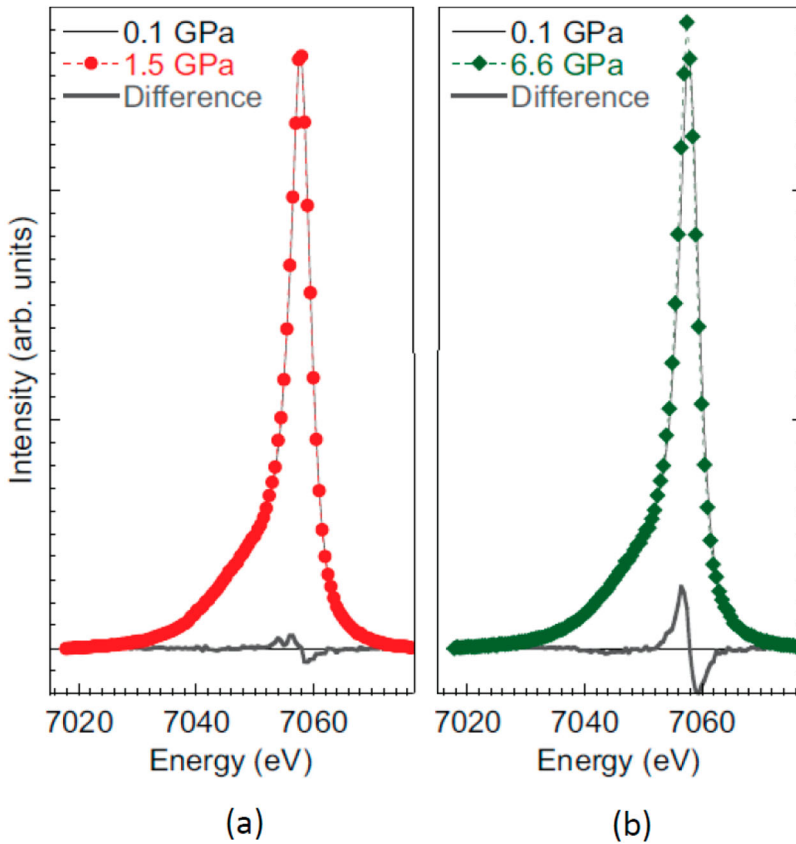


Figure 7. XES spectra of $(\text{Ca}_{0.67}\text{Sr}_{0.33})\text{Fe}_2\text{As}_2$ under room temperature and high pressure at (a) 1.5 and (b) 6.6 GPa when compared to the spectrum at ambient pressure. Black solid lines are the difference spectra (modified with permission from Figure 2 of ref. [29]).

constrain theoretical models.[36] PFY-XAS and XES have been widely used to study local magnetic moment, mixed-valence and multi-configuration of $4f$ and $5f$ metals and their compounds under high pressure.[37–40]

Similar to the K_β mainline for $3d$ transition metals, the L_{γ_1} ($4d \rightarrow 2p_{1/2}$) emission line contains a main peak and a satellite peak, which comes from the interaction between $4d$ and $4f$ electrons. Thus, the L_{γ_1} emission line is sensitive to the local moment of lanthanides.[41] Figure 8 shows measured and theoretically calculated Ce L_{γ_1} emission spectra across the γ - α volume collapse transition, which often serves as a testing ground for theoretical models treating f -electron correlations.[36] Special care was taken to make sure that the sample was pure-Ce metal inside the DAC with 3 mm Be gasket. The satellite peak of L_{γ_1} decreases 30% across the volume collapse. XES experimental results and new dynamical mean field theory calculations provided not only solid evidence to support the Kondo model in conjunction with previous measurements, but also a general experimental methodology to study relevant strongly correlated f -electron systems.

Because of its sharpening effect, PFY-XAS is very suitable to study mixed-valence properties or the multi-configurational nature of f electron systems, especially for actinides

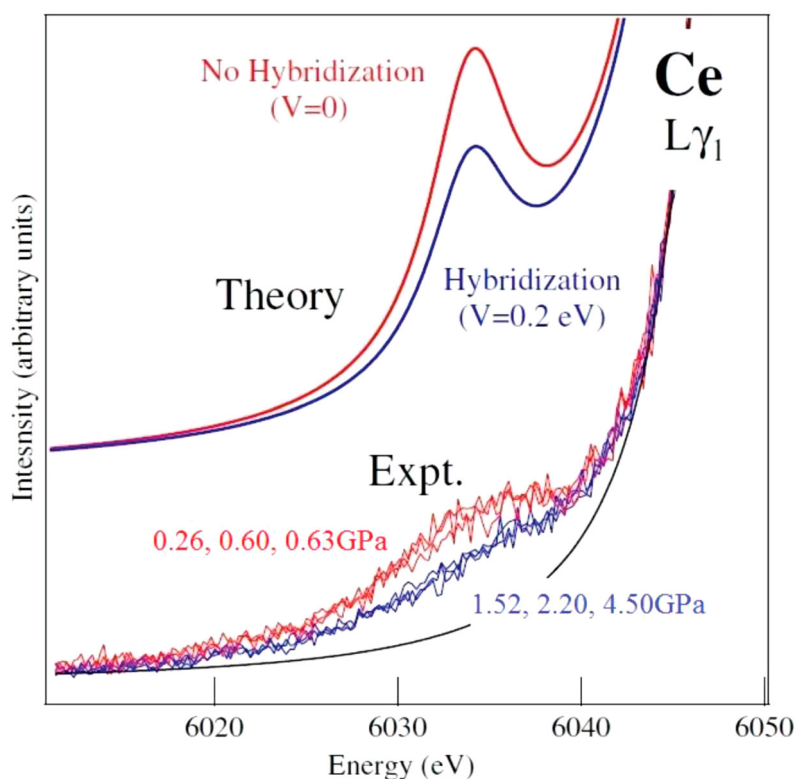


Figure 8. Satellite region of the Ce L_{γ_1} emission line as measured experimentally and calculated by the extended atomic model with and without hybridization (modified with permission from Figure 1 of ref. [36]).

where conventional XAS cannot resolve the fine distribution of the unoccupied electronic states due to the large lifetime broadening of the $2p_{3/2}$ level (~ 8 eV for Uranium).[42,43] Figure 9 plots PFY spectra at the Uranium L_{III} edge for the UCd_{11} compound at different pressures.[44] UCd_{11} is one of the most intriguing of all the binary uranium compounds and often used to study the effect of pressure on a strongly localized heavy-fermion intermetallic. An ~ 30 - μm -thick and 100 μm in diameter sample was loaded in the DAC with ruby chips and methanol–ethanol as pressure medium. With increasing pressure, the white line is shifted $+4.1$ eV at the highest measured pressure of 28.2 GPa. Both the white line shifting to higher energy and decreasing edge jump under compression indicate the delocalization of U $5f$ -electrons toward $6d$ band.

3.3. Valence band of Ge under high pressure

Valence-to-core XES (VtC-XES) probes electron transition from the valence band to the core level. Although known for many decades, extensive studies have become possible only in the late 1990s because of the very low transition probability.[5] VtC-XES can provide information similar to that of valence-band X-ray photoelectron spectroscopy (XPS) and can be used to probe electronic structure of ligand and valence-band

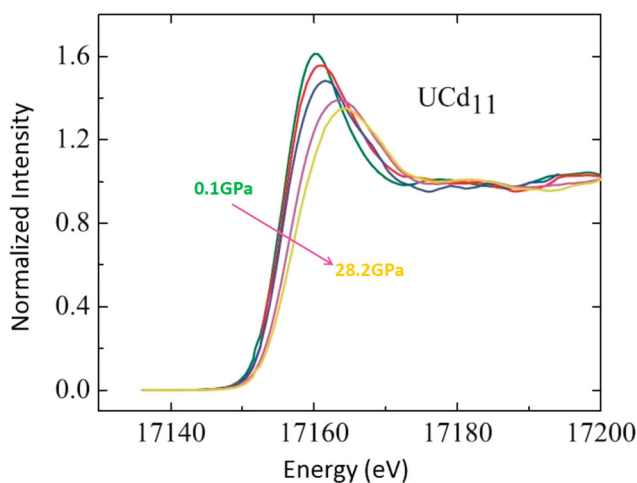


Figure 9. PFY-XAS spectra at the U L_{III} edge for UCd_{11} at different pressures (modified with permission from ref. [44]).

levels.[6,45] Although XPS has higher energy resolution, VtC-XES, as a hard X-ray technique, is element selective and can be used to probe samples under *in situ* or *in operando* environments for catalysis studies and for high pressure studies in which samples are embedded in gasket and anvil materials. With the advent of high-brightness third-generation synchrotrons and multi-crystal XES spectrometer collecting large solid angles, VtC XES has been applied to studies in the environment science, catalysis, bio-inorganic chemistry, and semiconductor fields.[46–49]

There are only a few high pressure studies involving VtC XES and two of them investigate the valence band of Ge.[27,50,51] The band structure is among the most important way to characterize the electronic structure of a solid and is responsible for various electrical properties of the material. Figure 10 plots the experimental width of the valence band (from FWHM of XES data) of Ge as a function pressure and compares it to previous experimental data and several density functional theory calculations.[51,52] Because of the sharpening effect of RXES, a change in valence band width was observed before the $\alpha \rightarrow \beta$ structural transition around 11 GPa. The valence band width increases slightly until 7.7 GPa due to the reduction of 4s character and decreases at higher pressure because of *d*-orbitals contribution. After the structural transition, the valence band width increases with increasing pressure. Both the electron density distribution and XES results show that the electronic structure changes at pressures far below the $\alpha \rightarrow \beta$ structure transition pressure and the existence of such pre-transition process may be common in other covalent-metallic phase transition.

4. An outlook

New diffraction-limited storage rings have ultra-low emittance in both horizontal and vertical directions (~ 50 pm-rad for APS-U) and can provide a much smaller and intense beam down to sub-micrometers.[53] In addition to the future higher brightness X-ray sources, technologies for making X-ray focusing mirrors have been much improved in recent

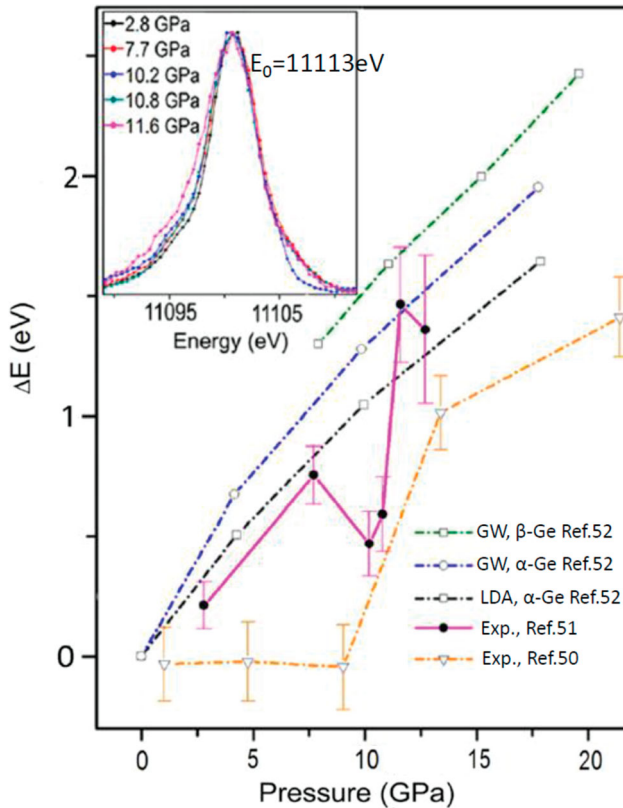


Figure 10. The FWHM of the XES data as a function of pressure (inset, $E_0=11,113$ eV) when compared to those of theoretical calculations from ref. [52] and the previous experiment result from ref. [50] (modified with permission from Figure 3 of ref. [51]).

years. Mirrors can be half a meter long and still have a very small slope error (<0.25 urad). Some mirrors can be made with a slope error less than 0.1 urad. The highest pressure in XES measurement so far is around 1.4 Mbar for FeO.[27] High pressure XES will greatly benefit from the developments in new synchrotron radiation sources and improved X-ray focusing optics. Multi-megabar XES experiments will become feasible because of the small and intense incident beam. The improved efficiency will also make XES mapping feasible.

It should be noted that the efficiency of the currently used XES spectrometers is still limited by the use of crystal analyzers to achieve the required energy resolution (\sim a few hundred meVs to a few eVs) that cannot be achieved by the detectors (either solid state detector or position-sensitive detector) used in those spectrometers. Recently, superconducting transition-edge sensors (TES) with high-energy resolution have been developed.[54] A single TES can reach an energy resolution of 1.6 eV FWHM at 6 keV, which is comparable to that of a typical XES spectrometer using a crystal analyzer.[55] Efforts are being made to construct arrays of TES to cover a large solid angle and increase counting efficiency.[56] Using such TES arrays for XES measurement will no longer require the use of crystal analyzers, dramatically simplifying the experimental setup. Moreover, using the TES arrays will eliminate the need of angle-analyzer scanning process, making

the highly efficient measurement suitable for time-resolved studies.[57,58] Even though the TES count rate limitation of a few hundred counts per second is a concern, high pressure XES is generally a low count rate technique due to small sample size and absorption of anvils and/or gasket. Therefore, using a TES array detector in high pressure XES will dramatically expand the XES capabilities for high pressure research, including position scanning imaging, time-resolved measurements, and multi-megabar measurements.

Acknowledgements

We would like to thank Dr Ravhi Kumar for providing high pressure RXES data in [Figure 3](#).

Disclosure statement

No potential conflict of interest was reported by the authors.

Funding

This work was performed at HPCAT (Sector 16), Advanced Photon Source (APS), Argonne National Laboratory. HPCAT operations are supported by DOE-NNSA under Award No. [DE-NA0001974] and DOE-BES under Award No. [DE-FG02-99ER45775], with partial instrumentation funding by NSF. The Advanced Photon Source is a U.S. Department of Energy (DOE) Office of Science User Facility operated for the DOE Office of Science by Argonne National Laboratory under Contract No. [DE-AC02-06CH11357].

References

- [1] Rueff JP, Kao CC, Struzhkin VV, et al. Pressure-induced high-spin to low-spin transition in FeS evidenced by X-ray emission spectroscopy. *Phys Rev Lett*. 1999;82:3284–3287.
- [2] Rueff JP, Shukla A. Inelastic X-ray scattering by electronic excitations under high pressure. *Rev Mod Phys*. 2010;82:847–896.
- [3] Dallera C, Annese E, Rueff JP, et al. Intermediate valence behaviour under pressure: how precisely can we probe it by means of resonant inelastic X-ray emission? *J Phys Condens Matt*. 2005;17:S849–S858.
- [4] Milne CJ, Penfold TJ, Chergui M. Recent experimental and theoretical developments in time-resolved X-ray spectroscopies. *Coordin Chem Rev*. 2014;277:44–68.
- [5] Glatzel P, Bergmann U. High resolution 1s core hole X-ray spectroscopy in 3d transition metal – electronic and structural information. *Coordin Chem Rev*. 2005;249:65–95.
- [6] Gallo E, Glatzel P. Valence to Core X-ray Emission Spectroscopy. *Adv Mater*. 2014;26:7730–7746.
- [7] Eisenberger P, Platzman PM, Winick H. Resonant X-ray Raman-scattering studies using synchrotron radiation. *Phys Rev B*. 1976;13:2377–2380.
- [8] de Groot FMF, Krisch MH, Vogel J. Spectral sharpening of the Pt L edges by high-resolution X-ray emission. *Phys Rev B*. 2002;66:195112.
- [9] de Groot FMF, Pizzini S, Fontaine A, Hamalaien K, Kao CC, Hastings JB. Local-spin-selective X-ray absorption and X-ray magnetic circular dichroism of MnP. *Phys Rev B*. 1995;51:1045–1052.
- [10] Xiao YM, Chow P, Boman G, et al. New developments in high pressure x-ray spectroscopy beamline at high pressure collaborative access team. *Rev Sci Instrum*. 2015;86:072206.
- [11] Sokaras D, Weng TC, Nordlund D, et al. A seven-crystal Johann-type hard x-ray spectrometer at the Stanford Synchrotron Radiation Lightsource. *Rev Sci Instrum*. 2013;84:053102.
- [12] Kleymenov E, van Bokhoven JA, David C, et al. Five-element Johann-type X-ray emission spectrometer with a single-photon-counting pixel detector. *Rev Sci Instrum*. 2011;82:065107.

- [13] Bergmann U, Cramer SP. A high-resolution large-acceptance analyzer for X-ray fluorescence and Raman spectroscopy. *Proc SPIE*. 1998;3448:198–209.
- [14] Szlachetko J, Cotte M, Morse J, et al. Wavelength-dispersive spectrometer for X-ray microfluorescence analysis at the X-ray microscopy beamline ID21 (ESRF). *J Synchrotron Rad*. 2010;17:400–408.
- [15] Mortensen DR, Seidler GT, Bradley JA, et al. A versatile medium-resolution x-ray emission spectrometer for diamond anvil cell applications. *Rev Sci Instrum*. 2013;84:083908.
- [16] Hoszowska J, Dousse JC. High-resolution XES and RIXS studies with a von Hamos Bragg crystal spectrometer. *J Electron Spec Relat Phen*. 2004;137:687–690.
- [17] Kallne E, Kallne J, Marmar ES, Rice JE. High-resolution X-ray spectroscopy diagnostics of high-temperature plasmas. *Phys Scrip*. 1985;31:551–564.
- [18] Hoszowska J, Dousse JC, Kern J, Rheme C. High-resolution von Hamos crystal X-ray spectrometer. *Nuc Instrum Methods A*. 1996;376:129–138.
- [19] Szlachetko J, Nachtegaal M, de Boni E, et al. A von Hamos X-ray spectrometer based on a segmented-type diffraction crystal for single-shot x-ray emission spectroscopy and time-resolved resonant inelastic X-ray scattering studies. *Rev Sci Instrum*. 2012;83:103105.
- [20] Alonso-Mori R, Kern J, Sokaras D, et al. A multi-crystal wavelength dispersive X-ray spectrometer. *Rev Sci Instrum*. 2012;83:073114.
- [21] Mattern BA, Seidler GT, Haave M, et al. A plastic miniature X-ray emission spectrometer based on the cylindrical von Hamos geometry. *Rev Sci Instrum*. 2012;83:023901.
- [22] Dickinson B, Seidler GT, Webb ZW, et al. A short working distance multiple crystal X-ray spectrometer. *Rev Sci Instrum*. 2008;79:123112.
- [23] Pacold JI, Bradley JA, Mattern BA, et al. A miniature X-ray emission spectrometer (miniXES) for high-pressure studies in a diamond anvil cell. *J Synchrotron Rad*. 2012;19:245–251.
- [24] Rueff JP, Mattila A, Badro J, Vanko G, Shukla A. Electronic properties of transition-metal oxides under high pressure revealed by x-ray emission spectroscopy. *J Phys Condens Matt*. 2005;17: S717–S726.
- [25] Lyubutin IS, Gavriluk AG, Struzhkin VV. High-spin–low-spin transition and the sequence of the phase transformations in the BiFeO₃ crystal at high pressures. *Jetp Lett*. 2008;88:524–530.
- [26] Lin JF, Struzhkin VV, Jacobsen SD, et al. Spin transition of iron in magnesiowustite in the Earth’s lower mantle. *Nature*. 2005;436:377–380.
- [27] Badro J, Struzhkin VV, Shu JF, et al. Magnetism in FeO at megabar pressures from X-ray emission spectroscopy. *Phys Rev Lett*. 1999;83:4101–4104.
- [28] Gretarsson H, Lupascu A, Kim J, et al. Revealing the dual nature of magnetism in iron pnictides and iron chalcogenides using X-ray emission spectroscopy. *Phys Rev B*. 2011;84:100509.
- [29] Jeffries JR, Butch NP, Lipp MJ, et al. Persistent Fe moments in the normal-state collapsed-tetragonal phase of the pressure-induced superconductor Ca_{0.67}Sr_{0.33}Fe₂As₂. *Phys Rev B*. 2014;90:144506.
- [30] Kumar RS, Zhang Y, Xiao Y, et al. Pressure induced high spin-low spin transition in FeSe superconductor studied by x-ray emission spectroscopy and ab initio calculations. *Appl Phys Lett*. 2011;99:012511.
- [31] Kumar RS, Zhang Y, Sinogeikin S, et al. Crystal and electronic structure of FeSe at high pressure and low temperature. *J Phys Chem B*. 2010;114:12597–12606.
- [32] Vanko G, Neisius T, Molnar G, et al. Probing the 3d spin momentum with X-ray emission spectroscopy: the case of molecular-spin transitions. *J Phys Chem B*. 2006;110:11647–11653.
- [33] Bauer ED, Thompson JD. Plutonium-based heavy-fermion systems, in: J.S. Langer (Ed.). *Ann Rev Condens Matt Phys*. 2015;6:137–153.
- [34] Gegenwart P, Steglich F, Geibel C, Brando M. Novel types of quantum criticality in heavy-fermion systems. *Euro Phys J*. 2015;224:975–996.
- [35] Steglich F, Arndt J, Stockert O, et al. Magnetism, f-electron localization and superconductivity in 122-type heavy-fermion metals. *J Phys Condens Matt*. 2012;24:294201.
- [36] Lipp MJ, Sorini AP, Bradley J, et al. X-ray Emission Spectroscopy of Cerium Across the gamma-alpha Volume Collapse Transition. *Phys Rev Lett*. 2012;109:195705.

- [37] Bradley JA, Moore KT, Lipp MJ, et al. 4f electron delocalization and volume collapse in praseodymium metal. *Phys Rev B*. 2012;85:100102.
- [38] Kumar RS, Svane A, Vaitheeswaran G, et al. Effect of pressure on valence and structural properties of YbFe₂Ge₂ heavy fermion compound—a combined inelastic X-ray Spectroscopy, X-ray diffraction, and theoretical investigation. *Inorg Chem*. 2015;54:10250–10255.
- [39] Rueff JP, Raymond S, Yaresko A, et al. Pressure-induced f-electron delocalization in the U-based strongly correlated compounds UPd₃ and UPd₂Al₃: Resonant inelastic X-ray scattering and first-principles calculations. *Phys Rev B*. 2007;76:085113.
- [40] Dallera C, Wessely O, Colarieti-Tosti M, et al. Understanding mixed valent materials: effects of dynamical core-hole screening in high-pressure x-ray spectroscopy. *Phys Rev B*. 2006;74:081101.
- [41] Jouda K, Tanaka S, Aita O. L gamma(1) and L beta(2,15) x-ray emission lines of rare-earth trifluorides and CeO₂. *J Phys Condens Matt*. 1997;9:10789–10794.
- [42] Kvashnina KO, Kvashnin YO, Butorin SM. Role of resonant inelastic X-ray scattering in high-resolution core-level spectroscopy of actinide materials. *J Electron Spec Relat Phen*. 2014;194:27–36.
- [43] Booth CH, Jiang Y, Wang DL, et al. Multiconfigurational nature of 5f orbitals in uranium and plutonium intermetallics. *Proc Nat Acad Sci*. 2012;109:10205–10209.
- [44] Nasreen F, Antonio D, VanGennep D, et al. High pressure effects on U L-3 X-ray absorption in partial fluorescence yield mode and single crystal X-ray diffraction in the heavy fermion compound UCd₁₁. *J Phys Condens Matt*. 2016;28:105601.
- [45] Pollock CJ, DeBeer S. Insights into the geometric and electronic structure of transition metal centers from valence-to-core X-ray emission spectroscopy. *Acc Chem Res*. 2015;48:2967–2975.
- [46] Eeckhout SG, Safonova OV, Smolentsev G, et al. Cr local environment by valence-to-core X-ray emission spectroscopy. *J Anal Atomic Spec*. 2009;24:215–223.
- [47] Bordiga S, Bonino F, Damin A, Lamberti C. Reactivity of Ti(IV) species hosted in TS-1 towards H₂O₂-H₂O Solutions investigated by ab initio cluster and periodic approaches combined with experimental XANES and EXAFS data: a review and new highlights. *Phys Chem Chem Phys*. 2007;9:4854–4878.
- [48] Lancaster KM, Roemelt M, Ettenhuber P, et al. X-ray emission spectroscopy evidences a central carbon in the nitrogenase iron-molybdenum cofactor. *Science*. 2011;334:974–977.
- [49] Szlachetko J, Michalow-Mauke K, Nachtegaal M, Sa J. Determination of conduction and valence band electronic structure of anatase and rutile TiO₂. *J Chem Sci*. 2014;126:511–515.
- [50] Struzhkin VV, Mao HK, Lin JF, et al. Valence band X-ray emission spectra of compressed germanium. *Phys Rev Lett*. 2006;96:137402.
- [51] Li R, Liu J, Bai L, Tse JS, Shen G. Pressure-induced changes in the electron density distribution in alpha-Ge near the alpha-beta transition. *App Phys Lett*. 2015;107:072109.
- [52] Modak P, Svane A, Christensen NE, Kotani T, van Schilfgaarde M. Pressure variation of the valence band width in Ge: a self-consistent GW study. *Phys Rev B*. 2009;79:153203.
- [53] Borland M, Decker G, Emery L, Sajaev V, Sun Y, Xiao A. Lattice design challenges for fourth-generation storage-ring light sources. *J Synchrotron Rad*. 2014;21:912–936.
- [54] Ullom JN, Doriese WB, Fischer DA, et al. Transition-edge sensor microcalorimeters for X-ray beamline science. *Synchrotron Rad News*. 2014;27:24–27.
- [55] Bandler SR, Adams JS, Bailey CN, et al. Advances in small pixel TES-Based X-Ray microcalorimeter arrays for solar physics and astrophysics. *IEEE Trans App Supercon*. 2013;23:2238752.
- [56] Ullom JN, Bennett DA. Review of superconducting transition-edge sensors for X-ray and gamma-ray spectroscopy. *Supercond Sci Tech*. 2015;28:084003.
- [57] Joe YI, O'Neil GC, Mijsa-Avila L, et al. Observation of iron spin-states using tabletop x-ray emission spectroscopy and microcalorimeter sensors. *J Phys B*. 2016;49:024003.
- [58] Uhlig J, Doriese WB, Fowler JW, et al. High-resolution X-ray emission spectroscopy with transition-edge sensors: present performance and future potential. *J Synchrotron Rad*. 2015;22:766–775.
- [59] Booth CH, Durakiewicz T, Capan C, et al. Electronic structure and f-orbital occupancy in Yb-substituted CeCoIn₅. *Phys Rev B*. 2011;83:235117.